Tri-band Millimetre-wave Antenna for Body-centric Networks

Masood Ur-Rehman*, Michael Adekanye, and Hassan Tariq Chattha

University of Bedfordshire, Luton LU1 3JU, United Kingdom

Islamic University Madinah, Kingdom of Saudi Arabia

Abstract

This paper presents design of a tri-band slotted patch antenna operating at millimeter-wave frequencies of 28 GHz, 38 GHz and 61 GHz. The proposed antenna carries an overall size of $5.1mm \times 5mm \times 0.254mm$ employing a single layer, slotted patch structure combining L- and F-shaped slots. It is excited by a single-feed microstrip line. The antenna is tested in free space as well as in wearable configurations and results show that it offers a good impedance matching, sufficient -10 dB bandwidth and wide radiation coverage at the three bands of interest effectively countering the effects of human body presence. It achieves a peak gain of 7.2 dBi in off-body and 8.3 dBi in on-body configuration. Minimum efficiency values are observed to be 85% in off-body while 54% in on-body scenarios. A comparative analysis with published relevant work shows that the proposed antenna is inexpensive, easy to integrate and works efficiently in tri-band wearable and implantable arrangements. These features make it a good candidate for current and future applications of Body-centric Networks operating at millimeter-wave ranges.

Keywords: Body-centric Networks, Millimeter-waves, Microstrp patch antenna, Multi-band antenna, 5G communications.

*Corresponding author

Email address: masood.urrehman@beds.ac.uk (Masood Ur-Rehman)

1. Introduction

The demand for wireless communications has increased by multiple folds in recent years due to advent of wearable sensors and Internet-of-Things (IoT). Body-centric Networks (BCNs), that make use of in-body, on-body and near-body communication devices to gather, process and transmit vital information, have seen a massive growth as a result. These networks have a wide variety of applications ranging from healthcare to infotainment and navigation to sports [1, 2, 3]. Their popularity is such that estimates suggest a demand of 187.2 million wearable units annually by 2020 [4, 5]. This along with high drive for increased network capacity and data rates has put a great amount of pressure on the present Fourth Generation (4G) wireless communication systems. The wireless technology is therefore, aiming to make its Fifth Generation (5G) operational by 2020 where millimetre-wave (mm-Wave) frequency bands of 28 GHz/38 GHz are potential candidates for the cellular communications while 60 GHz band is spotted as the front-running contender for the BCNs [1, 6, 7]. Millimeter-wave is attracting much interest as it offers a number of benefits including smaller and light weight components, wide bandwidth, high data rate and low interference to name a few [8].

Efficient design and implementation of BCNs depend highly on the working of antenna. Design of such antennas is very challenging due to added requirements of having low profile, light weight, low power consumption and flexibility on top of typical specifications of impedance matching, bandwidth, radiation pattern, efficiency and gain [9, 10]. Another aspect that needs careful considerations is impact of human body presence on the performance of these antennas as the human user is an integral part of BCNs [3]. It is a well established fact that presence of the human body in the vicinity of antennas introduces losses by detuning frequency and distorting radiation pattern as a result of electromagnetic absorptions in human body tissues and reflections/scattering from the body surface [3, 11, 12]. These effects are well-characterised at the lower operational frequencies but mm-Wave frequencies need in-depth investigations

[1, 3, 13, 14, 15]. It is also important to design an antenna with higher gain at mm-Wave frequencies to subdue increased levels of path loss [16].

Design of mm-Wave antennas have received good degree of interest from the researchers. A number of studies have considered antenna design at 28 GHz, 38 GHz and 60 GHz frequencies [17, 18, 19, 20, 21, 22, 23, 24, 25, 26]. A 2×2 patch array using low-temperature cofired ceramic (LTCC) technology is presented in [17]. Single element consists of two circular patches with diagonal perturbations. A planar parallel stripline feeding network has been used to feed the array covering frequencies of 30-40 GHz with a maximum gain of 9.3 dBi. A dual-feed square loop antenna is proposed by Li et al. in [18]. The antenna operates at 38.5 GHz and offers a peak gain of 2.9 dBi. A scaled version to operate at 73.5 GHz is also discussed by the authors. A 3×3 series-fed patch array for 28 GHz band is presented in [19]. The patches are connected to each other in series and 2-D symmetric formation using high-impedance microstrip lines provides a gain of 14.9 dBi. Aliakbari *et al.* have proposed a single-fed circular polarised antenna for dual-band operation at 28 GHz and 38 GHz bands [20]. The antenna makes use of a composite structure combining two L-shaped slots etched on a square patch and achieves a peak gain of 4.5 dBi at at 38 GHz. A proximity-fed elliptical patch etched non-concentrically in an elliptical slot located at the antenna ground plane is used for dual-band operation at 28 GHz/38 GHz in [21]. An L-shaped slot is etched off in the feed line to create separation between the two bands. The antenna has a peak gain of 4.4 dBi.

A four-element linear array antenna working at 28 GHz/38 GHz bands fed via 1×4 Wilkinson power divider is discussed in [22]. The antenna employs a slotted Substrate Integrated Waveguide (SIW) array structure and Electromagnetic Band Gap (EBG) ground plane to attain a peak gain of 11.9 dBi at 28 GHz. Xie *et al.* have designed a Dielectric Resonator Antenna (DRA) array with a 8-way Wilkinson power divider as the feed network [23]. The unit cell has a semi-cylindrical dielectric loaded on a rectangular patch. The array works at 28 GHz with a maximum gain of 15 dBi. A disc-like antenna having an electromagnetic coupling between a circular disc and the feeding pin is considered

in [25]. This antenna is using substrate integrated horn for the feeding. Lu *et al.* have used three-stage ladder-shaped directors to enhance the directivity by 2.4-3.1 dB and bandwidth by 30% of a four-arm quasi-Yagi antenna [24]. A patch antenna on a Flexible Printed Circuit Board (FPCB) for 60 GHz BCNs operation is discussed in [26]. This antenna employs an air gap between two layers of the FPCB to achieve a bandwidth of 9.8 GHz and offers a gain of 10.6 dBi in off-body (free space) configuration.

Most of these antennas employ complex geometries, array structures and require difficult feeding arrangements. Moreover, very few of these studies consider the antenna performance in wearable scenarios limiting their applicability in BCN applications. We have, therefore, attempted to design a low profile and efficient antenna for BCNs operating at mm-Wave frequencies in this paper. Since, a multi-band approach is envisaged as useful in maintaining small form factor while achieving a multi-frequency operation, the proposed antenna employs a simple slotted-patch geometry fed through a microstrip line to cover three popular bands of 28 GHz, 38 GHz and 61 GHz. The performance of the proposed antenna in off-body, on-body and in-body scenarios is investigated through numerical analysis. The simulated results are verified through measurements. Efficient antenna performance in terms of impedance bandwidth and radiation characteristics in all three scenarios make it a potentially viable solution for tri-band mm-Wave BCNs.

Following the introduction in this section, rest of this paper is organised in four sections. Design of the proposed antenna with detailed parametric study is presented in Section II. Section III discusses performance of the antenna in free space and wearable scenarios while conclusions are drawn in Section IV.

2. Antenna Design

2.1. Concept and Topology

Requirements of low profile, simple geometry, ease of integration and low cost for the BCN antennas make a patch-type structure one of the most feasible

solutions. Such antennas usually have a ground plane that helps to minimise backward radiations towards the human user. On the other hand, substrate thickness provides a gap between the radiating element and the human user helping to slightly reduce the degrading effects on impedance matching and antenna efficiency [26]. A patch geometry combining a square patch and L- and F-shaped slots positioned close to edges of the patch is therefore, used as a radiator in the proposed antenna. This arrangement results in inductive and capacitive effects which generates the multi-frequency operation.

The antenna uses Rogers RT/ Duroid 5880 printed circuit board with a thickness of 0.254 mm. Substrate has a relative permittivity of 2.2 and $tan\sigma$ = 0.0009. RT/ Duroid 5880 is suitable for high-frequency operation because of low dielectric loss minimising losses and dispersion at these frequencies [27]. The antenna is fed through a 50 Ω microstrip feed line and overall size of the antenna is 5.1×5×0.254 mm^3. The antenna is modelled and simulated using CST Microwave Studio® that employs Finite Integration Technique (FIT) to solve the Maxwell's equations [28]. Geometry and dimensions of the modelled antenna are shown in Figure 1.

Addition of the L- and F-shaped slots to the square patch together with off-centered microstrip feed improves impedance matching while reducing the overall size of the patch. The three structures also generate resonances at the three operating bands. A major portion of the antenna radiation comes from the slots. The current is mostly concentric on the edges of the patch and slots as evident from Figure 2. It also shows that the microstrip line provides feed balancing.

2.2. Parametric Study

Optimisation of various structural parameters is necessary to realise an antenna structure having good impedance matching and radiation characteristics. Effects of three key elements including width of the slots, length of notch 1 and length of notch 3 (refer to Figure 1) on the performance of the proposed antenna are investigated to better understand the antenna operating principle.

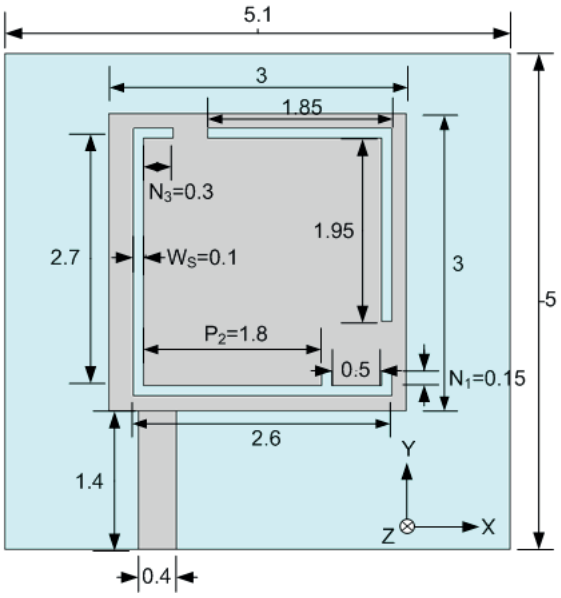

(a) Front view

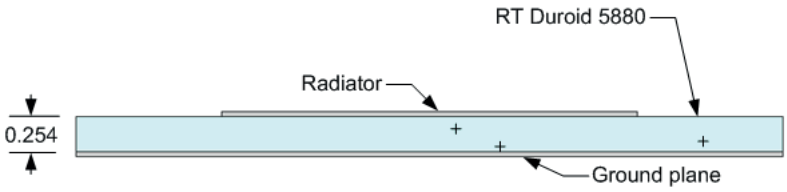

(b) Side view

Figure 1: Geometry and dimensions of the proposed tri-band antenna (all units are in mm).

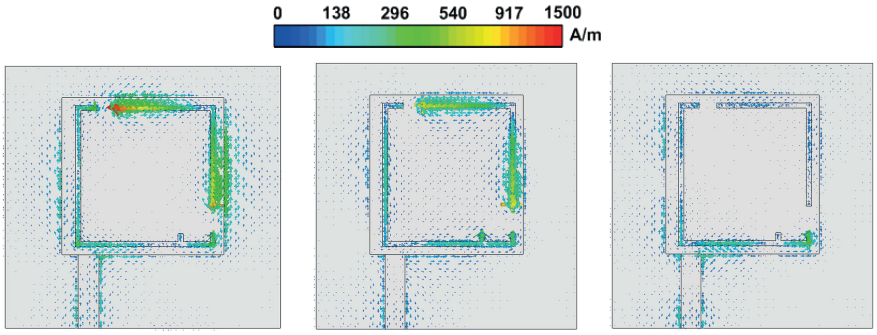

(a) 28 GHz (b) 38 GHz (c) 61 GHz

Figure 2: Surface current distribution on the proposed antenna at 58 GHz, 60 GHz and 62 GHz.

Optimised values are taken as a reference.

2.2.1. Width of the Slots (W_s)

Width of L- and F-shaped slots is one of the key design elements. Its impact on the impedance matching and bandwidth in terms of reflection coefficient (S_{11}) is studied and presented in Figure 3. These results show that change in the width of the slots has a very profound effect on the impedance matching and bandwidth of the antenna. Narrower slots (W_s=0.05 mm) reduces the gap between 28 GHz and 38 GHz bands while losing operation completely at 61 GHz. Wider slots (W_s=0.2 mm) on the other hand, brings an opposite change by increasing the gap between the two lower frequencies and a better matching at 61 GHz. Wider slots however, tend to loose matching at 38 GHz.

2.2.2. Length of Notch 1 (N_1)

Length of notch 1 also plays an important role in the antenna performance. Effects of changing this parameter is compared with the optimal value of N_1=0.15 in terms of S_{11} in Figure 4. The results show that this parameter is vital for the tri-band operation of the antenna. Any change in N_1 not only varies the bandwidth by shifting the resonance but also affects the impedance matching. A shorter notch improves the matching at 28 GHz with slight upward shift of the

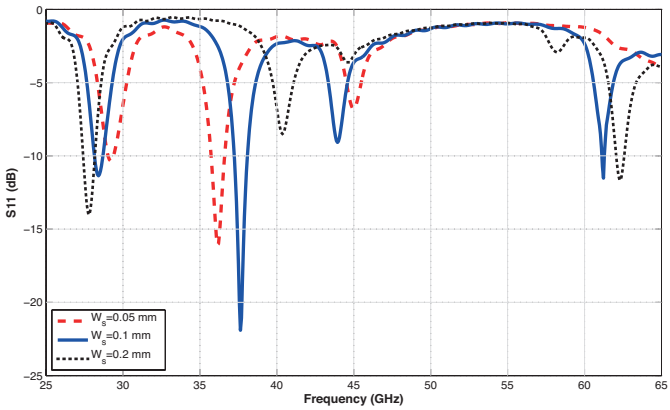

Figure 3: Effects of width of the slots on the performance of the proposed antenna.

resonance and increase in the bandwidth at the expense of -10 dB bandwidth at the two higher bands. On contrary, a larger notch improves the matching but undergoes a downward resonance shift that is more significant at 61 GHz band.

2.2.3. Length of Notch 3 (N_3)

Influence of the length of notch 3 on the antenna performance is depicted through reflection coefficient response in Figure 5. Role of this parameter is also important in the matching and bandwidth but does not impact the tri-band operation as significantly as notch 1. A reduced length of (N_3) improves the matching at the three bands but with an upward shift in the resonance at 61 GHz. A larger notch 3 looses the matching at 28 GHz and 61 GHz but maintains the performance at the middle band.

3. Antenna Performance

Impedance and radiation characteristics of the proposed mm-Wave antenna are studied in off-body (free space) and wearable configurations throughout the range of the operating frequencies in terms of reflection coefficient response, radiation patterns, peak gain and radiation efficiency. Free space results are verified through measurements of fabricated prototype of the antenna. These

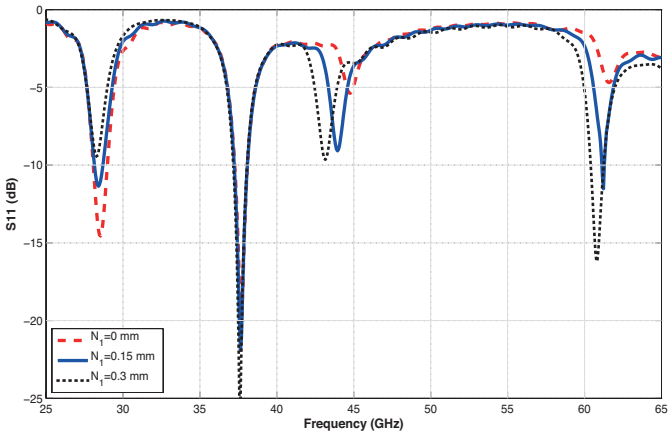

Figure 4: Effects of length of the notch 1 on the performance of the proposed antenna.

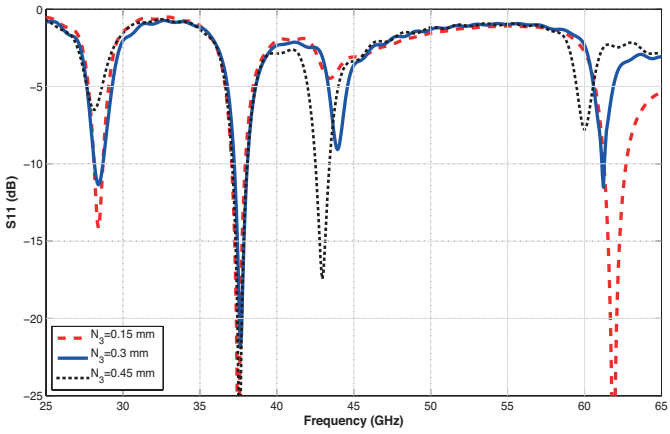

Figure 5: Effects of length of the notch 3 on the performance of the proposed antenna.

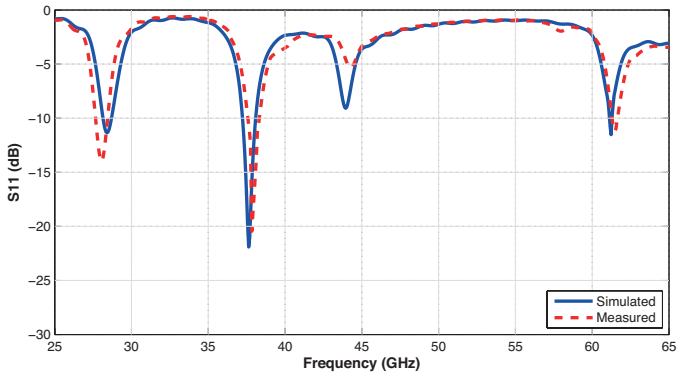

Figure 6: Simulated and measured reflection coefficient response of the proposed antenna.

measurements are taken in an anechoic chamber using Anritsu's MS4647B Vector Network Analyser (VNA).

3.1. Off-body Scenarios

This section discusses the antenna results being observed in off-body (free space) scenarios.

The simulated and measured reflection coefficient response of the proposed antenna is given in Figure 6. The results show that the antenna achieves a good impedance matching at the three bands for the tri-band mmWave operation. It also exhibits good -10 dB bandwidth of 840 MHz, 370 MHz and 900 MHz at 28 GHZ, 38 GHz and 61 GHz, respectively. A good agreement between simulation and measurement is observed. Discrepancies are associated to fabrication imperfections and spurious radiations from coaxial cable and connector.

Figure 7 compares the measured and simulated antenna radiation patterns at $\phi = 0^o$ and $\phi = 90^o$ at the three operating frequencies. A good radiation coverage with nearly omni-directional pattern can be observed from these results. Higher frequency band brings slight distortions in $\phi = 90^o$ pattern as expected. The simulation results agree well with the measurements.

Comparison of the simulated and measured peak gain and radiation efficiency of the antenna at the three mm-Wave bands of interest is presented in Figure

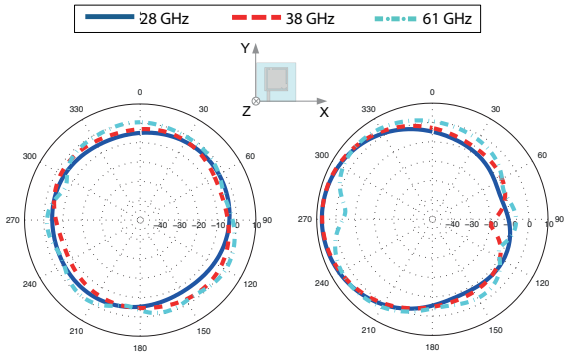

(i) $\phi = 0^o$ (ii) $\phi = 90^o$

(a) Simulated

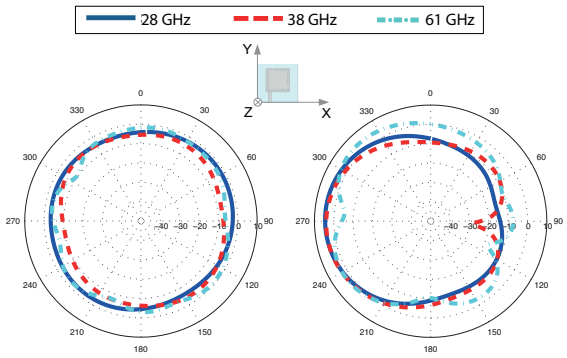

(i) $\phi = 0^o$ (ii) $\phi = 90^o$

(b) Measured

Figure 7: Simulated and measured radiation patterns of the proposed tri-band antenna at three bands of interests of 28 GHz, 38 GHz and 61 GHz.

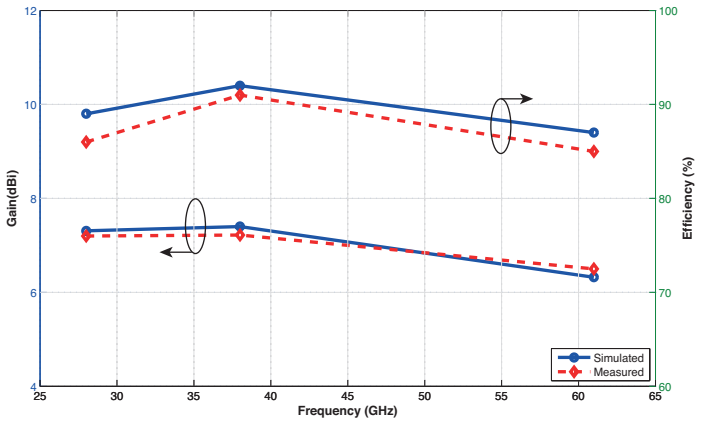

Figure 8: Simulated and measured gain and efficiency values for the proposed antenna.

8. The antenna achieves maximum gain of 7.4 dBi in simulation and 7.22 dBi in measurement at 38 GHz. Minimum gain is being observed at 61 GHz with values of 6.32 dBi in simulation and 6.5 dBi in measurement.

A similar trend is noted for the antenna efficiency. Efficiency values are 89%, 92% and 87% in simulation at 28 GHz, 38 GHz and 61 GHz, respectively. Measured efficiency values appear to be 86%, 91% and 85% at the three bands, respectively. A good agreement between the measured and simulated values is also evident.

3.2. Wearable Scenarios

The human user is an integral part of the BCNs whose presence brings severe distortions in the antenna performance. Implanted sensors is also one of the fast growing BCN applications. It is therefore, essential to analyse the BCN antennas in potential body-worn scenarios. This section presents a detailed investigation on the antenna impedance and radiation characteristics in on-body and in-body (implanted) configurations to establish its usability for BCN applications.

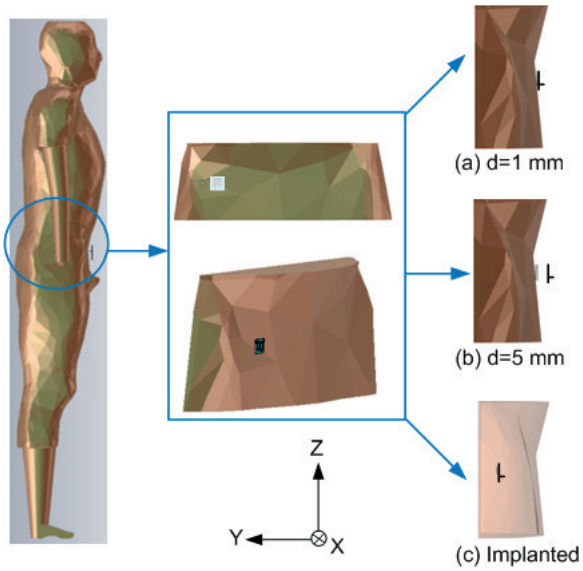

Figure 9: Structure of the realistic skin-equivalent human phantom taken out of a high-resolution human body model.

3.2.1. Numerical Modelling of Skin Phantom

Maximum electromagnetic absorption by the human body at mm-Wave frequencies takes place in the skin tissues due to a penetration depth of around 0.5 mm. A single layer homogeneous torso phantom with electric properties of dry skin is therefore, used in this investigation to study the effects of human body presence on the performance of the proposed tri-band antenna.

The skin-equivalent torso phantom has a realistic organ shape as it has been taken out of a high resolution whole-body model as shown in Figure 9. Overall dimensions of the phantom are $288 \times 100 \times 40\ mm^3$. An adaptive meshing scheme is used to reduce the overall number of cell volumes (voxels) in the computational domain. It helps to reduce the computation time for the model. The Perfectly Matched Layer (PML) absorbing boundary conditions are used [28]. The model has a maximum resolution of 2 mm near the boundaries of the computational domain.

Dielectric properties of the dry skin tissue up to a frequency of 110 GHz has

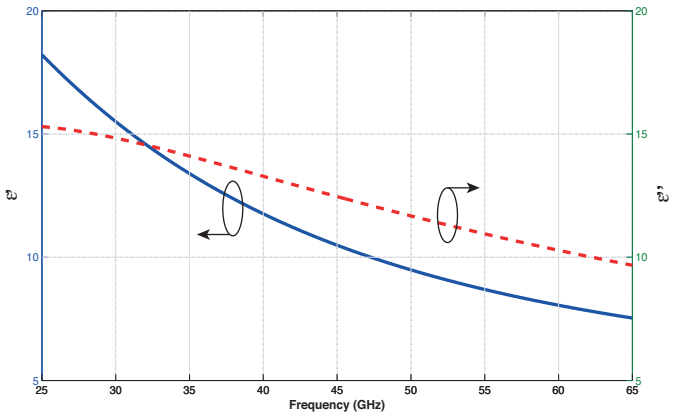

Figure 10: Complex permittivity of dry skin in 25 GHz-65 GHz band.

been well characterised through extrapolation of experimental data measured up to 20 GHz [29, 30]. Debye model with a single relaxation time is used to model the permittivity data with good level of accuracy to the measured values in our frequency range of interest [31]:

$$\varepsilon^* = \varepsilon_o(\varepsilon^{'} - j\varepsilon^{''}) = \varepsilon_o(\varepsilon_\infty + \frac{\varepsilon_s - \varepsilon_\infty}{1 + j\omega\tau}) \quad (1)$$

where ε_o is the free space permittivity ($8.85{\times}10^{-12}$ F/m), ε_s represents the static permittivity, ε_∞ is the optical permittivity, ω depicts the angular frequency and τ is the relaxation time. Optimised values for the best fit in the frequencies of interest are: $\varepsilon_s = 34.8$, $\varepsilon_\infty = 4.1$ and $\tau = 6.9 \times 10^{-12}$ [32]. Modelled permittivity values are plotted in Figure 10.

3.2.2. Results and Discussion

Two typical body-worn scenarios and one implanted configuration are studied. The considered body-worn scenarios include placement of the antenna at a gap of 1 mm (d=1 mm) from the surface of the phantom to replicate antenna placed directly on-body and a gap of 5 mm (d=5 mm) to incorporate clearance for the casing of the BCN device as shown in Figure 9. For the in-body

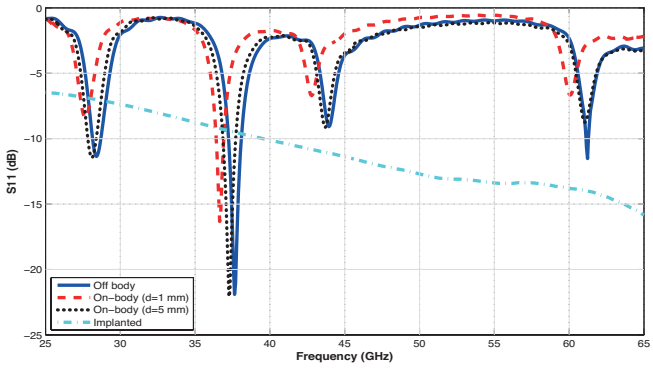

Figure 11: Reflection coefficient response of the proposed antenna in wearable and implantable scenarios in comparison with free space performance.

(implanted) scenario, antenna is placed into the skin phantom at a depth of 20 mm.

Reflection coefficient responses and radiation patterns of the proposed antenna at the three operating frequencies in the off-body (free space), on-body and implanted scenarios are compared numerically and illustrated in Figures 11 and 12. These results show that the antenna is quite resilient to the effects of human body presence. Though, the presence of the phantom introduces impedance mismatch and detuning, the antenna successfully keeps its operation intact at 38 GHz for all on-body scenarios. The d=1 configuration affects the matching and reduces the bandwidth at the three frequencies very significantly. The impact is more drastic at 28 GHz and 61 GHz band where the matching is reduced to -6 dB due to change in electrical properties of the substrate. Resonance shift and mismatch is minimal at all three bands when antenna is placed at d=5 mm. The antenna performance is significantly affected when implanted in the body as matching is changed completely due to the presence of a high volume of body tissues. Operation at 28 GHz is the worst affected but the antenna has retained -6 dB impedance matching which can be used in most of the commercial applications.

A similar trend is being observed for the antenna radiation pattern. The d=1

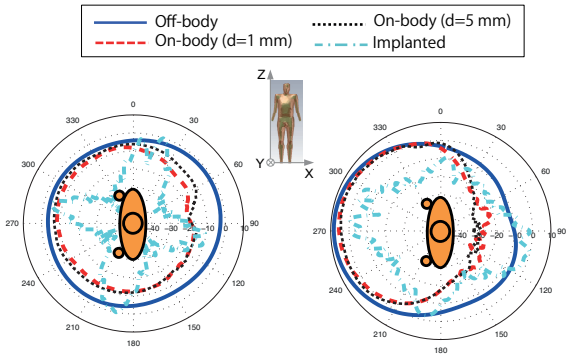

(i) $\phi = 0^o$ (ii) $\phi = 90^o$

(a) $f = 28GHz$

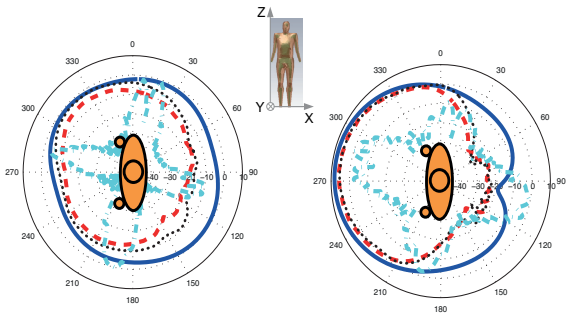

(i) $\phi = 0^o$ (ii) $\phi = 90^o$

(b) $f = 38GHz$

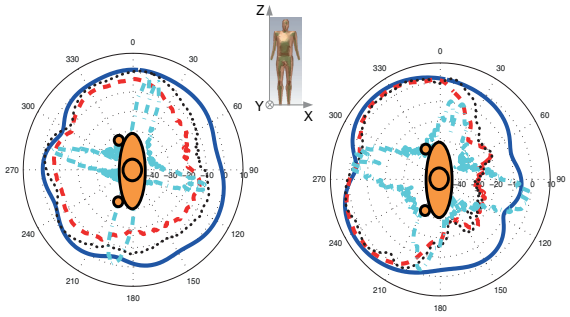

(i) $\phi = 0^o$ (ii) $\phi = 90^o$

(c) $f = 61GHz$

Figure 12: Radiation patterns of the proposed tri-band antenna in wearable and implantable scenarios at 28 GHz, 38 GHz and 61 GHz.

mm configuration affects the radiation more out of the two on-body scenarios due to higher reflections from the body surface. Level of the pattern distortion reduces for d=6 mm. In on-body placements, the human body backscatters energy changing induced current on the antenna structure, lowering back radiations due to absorptions and increasing maximum gain. In the implanted configuration, the antenna loses its directivity completely due to presence of the body mass in all directions. High absorptions are also visible. Overall, the radiation pattern is degraded more in $\phi = 0^o$ plane due to presence of higher body mass.

The peak gain values are observed to be 8.1 dBi, 8.3 dBi and 7.5 dBi at 28 GHz, 38 GHz and 61 GHz for d=1 mm, while 7.2 dBi, 7.9 dBi and 7.6 dBi for d=5 mm placements, respectively. These values are 13.3 dBi, 14 dBi and 14.3 dBi for the implanted configuration. The antenna radiation efficiency in the presence of the human body also decreases due to absorptions in the lossy human body tissues. Simulated efficiency varies from 54%, 60% and 58% for d=1 mm to 55%, 62% and 60% for d=5 mm at the three frequencies, respectively. In implanted situation, efficiency is observed to be 12%, 14% and 10%.

Specific Absorption Rate (SAR) averaged over 1 g of the body tissue volume for the proposed antenna having 0.5 W (peak) incident power has been evaluated to assess the level of exposure. For d=1 mm, peak SAR values are noted to be 14.6 W/kg, 13.9 W/kg and 18.1 W/kg while for d=5 mm, these values are observed to be 3.1 W/kg, 2.5 W/kg and 4.4 W/kg at 28 GHz, 38 GHz and 61 GHz, respectively. In the implanted configurations, SAR values are noted to be 310 W/kg, 280 W/kg and 332 W/kg.

These results show that in typical wearable configurations, the proposed antenna can work very well. It is therefore, suitable for body-worn applications where antenna is mounted on the circuit board or on top edge of the sensor/device. Implanted configurations need further exploration as to the best of our knowledge, no results at these frequencies are currently reported.

3.3. Comparison

The proposed antenna design is compared with related mm-Wave antennas reported in open literature, [17, 18, 20, 21, 22], in terms of structure, size and radiation characteristics to show its effectiveness. Particular emphasis is given to multi-band solutions. Table 1 presents a summary of this comparative study.

It is evident that the proposed antenna exhibits a tri-band operation with gain and efficiency values higher than most of the available designs. Solutions that offer better gain employs complex array structures. Moreover, the presented antenna makes use of a simple geometry offering ease of fabrication via traditional low cost techniques. It also has a size smaller than most of the reported designs except [21]. Furthermore, the proposed antenna works excellently in body-mounted configurations. This comparison clearly shows the advantages of the proposed antenna for mm-Wave BCN applications at 28 GHz, 38 GHz and 61 GHz bands.

4. Conclusion

A novel slotted patch antenna is presented for the BCN operation at millimetre-wave frequency bands of 28 GHz, 38 GHz and 61 GHz. The proposed antenna has a simple structure and low profile. It consists of a square patch having an L- and F- slot for the tri-band operation. The antenna has been tested for off-body (free space), on-body and implanted configurations. It has achieved a good bandwidth of 840 MHz, 370 MHz and 900 MHz at the three frequencies, a peak gain of 7.22 dBi at 38 GHz and radiation efficiency of 91% with good radiation coverage in off-body scenario. A good agreement between the simulated and measured results has been observed.

Though experiencing detuning, pattern degradation and drop in the efficiency in the on-body and implanted configurations, the antenna has performed excellently when positioned at a distance of 5 mm from the human body surface replicating typical body-worn scenarios. The antenna has achieved a maximum gain of 8.3 dBi and radiation efficiency of 60% in on-body placements. It

has undergone severe distortions when implanted inside the human phantom. However, it has succeeded to keep the impedance matching at 38 GHz and 61 GHz bands. SAR levels are also noted to be in line with the values reported in literature. Consequently, this low profile antenna is a good candidate for body-centric wireless devices operating at millimetre-wave frequencies. Future aspects of this work include measurements for on-body scenarios using human subjects and implanted scenarios using liquid phantoms and animals.

Table 1: Comparison between the proposed antenna and state-of-the-art mm-Wave antennas.

Parameter	Ref.					
	[17]	[18]	[20]	[21]	[22]	This work
Structure	LTCC array	Dual-feed square loop	L-slot	Slotted patch	SIW array	L- and F-slot
Size (mm)	15.3×28.3 ×1.3	30×15 ×0.254	6.8×6.8 ×0.254	5×5 ×0.127	27.5×20 ×0.254	5.1×5 ×0.254
Operating frequency (GHz)	29.7-40	38.5	28 38	28 38	28 38	28 38 61
-10 dB BW (GHz)	10.3	4.6	0.85 0.75	5 6	0.32 1.9	0.84 0.37 0.9
Off-body gain (dBi)	9.3	2.9	4 4.5	3.6 4.4	11.9 11.2	7.2 7.22 6.5
On-body gain (dBi)	N/I *	N/I *	N/I *	N/I *	N/I *	8.1 8.3 7.5
Off-body efficiency(%)	50	90	N/R **	N/R **	N/R **	86 91 85
On-body efficiency(%)	N/I *	N/I *	N/I *	N/I *	N/I *	54 60 58

* The paper does not investigate human body effects on the antenna.

** The authors have not reported this value.

References